A CMOS instrumentation amplifier designed with open-source tools

Cristina Missel Adornes, Gabriel Maranhão, Deni Germano Alves Neto,
Cesar Ramos Rodrigues, Márcio Cherem Schneider
Department of Electrical and Electronics Engineering
Federal University of Santa Catarina,
Florianópolis, SC, Brazil

***Abstract*—This paper presents a CMOS instrumentation amplifier based on a fully differential difference amplifier (FDDA) as part of a bioimpedance readout circuit for skin cancer detection. Developed using the open-source SkyWater 0.13 μm CMOS process from design to tape-out, the FDDA achieves a DC gain of 72 dB, a gain-bandwidth product of 47.8 MHz, an input-referred noise of 0.275 $\mu V/\sqrt{Hz}$ at 1 kHz, and a CMRR of 119.9 dB. This work highlights the potential of open-source design flows in developing high-performance FDDA circuits, paving the way for more accessible development of advanced biomedical applications.**

***Index Terms*—CMOS Instrumentation Amplifier, Fully Differential Difference Amplifier, Open-Source, Bioimpedance Readout, Integrated Circuit**

I. Introduction

Bioimpedance is a non-invasive technique that can be used for early detection of skin cancer. By measuring the electrical impedance of skin tissues, it is possible to differentiate between benign and malignant lesions based on their distinct electrical properties [1]. This research adopts a 4-electrode configuration for bioimpedance measurement, in which two electrodes inject a differential current into the body, while the other two measure the resulting voltage. The readout system in Figure 1 calculates the magnitude and phase of the bioimpedance transfer function from the measured voltage. This configuration minimizes synchronization issues and reduces circuit complexity [2], [3].

The measurement circuit uses two instrumentation amplifiers (INAs). The first INA measures the differential voltage between the sensing electrodes, while the second measures the voltage across a current-sense resistor (RI-SENSE). The phase detector converts these voltages into square waves and generates a pulse representing the phase difference between the two amplifier outputs. An integrator then produces a sawtooth waveform proportional to this phase difference. The system also includes a peak detector, which measures the magnitude of the signal from the first INA using a full-wave rectifier followed by a low-pass filter.

To implement this system, an INA based on fully differential difference amplifier (FDDA) was designed using an open-source design flow with the SkyWater 0.13 μm CMOS process. This demonstrates that high-performance bioimpedance circuits can be created using open-source tools from design to tape-out. The FDDA-based INA plays a key role in amplifying the small differential signals required for accurate bioimpedance measurements.

The remainder of this paper is organized as folllows: Section II presents the FDDA-based INA. Section III discusses post-layout simulation results and compares them to state-of-the art designs. Finally, Section IV concludes the paper with key remarks.

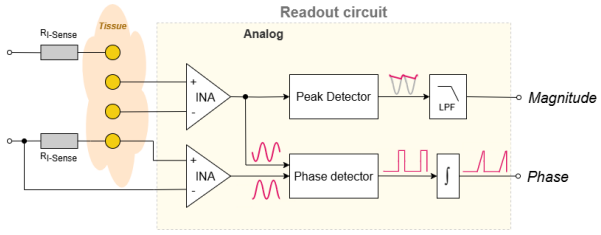

Fig. 1. Diagram of the magnitude/phase measurement system

II. FDDA-Based Instrumentation Amplifier

The INA is responsible for the initial amplification of small differential signals from the skin electrodes with minimal distortion and noise over a large frequency bandwidth. This performance ensures that the subsequent signal processing stages can accurately measure the bioimpedance magnitude and phase to distinguish between benign and malignant skin lesions.

Fully differential difference amplifiers simplify many application structures while improving noise rejection, dynamic range, and harmonic distortion of analog and mixed-signals systems [4], [5]. The FDDA-based INA eliminates the need for the input signal source to match the DC voltage at the output, as required by conventional INAs. Figure 2 shows the FDDA-based INA configuration, in which the closed loop gain is given by

$$\frac{v_{od}}{v_{id}} = 1 + \frac{R_2}{R_1} \tag{1}$$

The gain of the INA is determined by the resistor ratio $K_R = R2/R1$, allowing for adjustable and re-configurable

979-8-3315-2212-4/25/$31.00 ©2025 IEEE

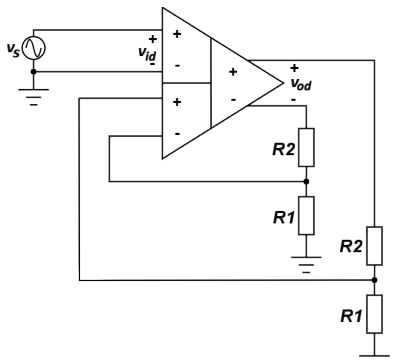

Fig. 2. FDDA-based instrumentation amplifier.

gain as needed. To ensure stable amplification across the 10 kHz to 1 MHz frequency range necessary for bioimpedance signals, the FDDA circuit requires a high gain-bandwidth product (GBW). Additionally, low input-referred noise, high common-mode rejection ratio (CMRR), and a high power supply rejection ratio (PSRR $>$ 60 dB) are critical to minimize interference and maintain signal integrity in the presence of power supply noise.

A. FDDA circuit

Figure 3 presents the FDDA scheme, which is a modified version of the single-ended design in [6], combined with a fully differential folded cascode amplifier. The folded cascode structure was chosen for its high gain and improved frequency response compared to conventional two-stage operational amplifiers. Additionally, the folded cascode amplifier allows for a higher common-mode input range and output-voltage swing than most amplifiers. However, its main drawback is an increased current consumption.

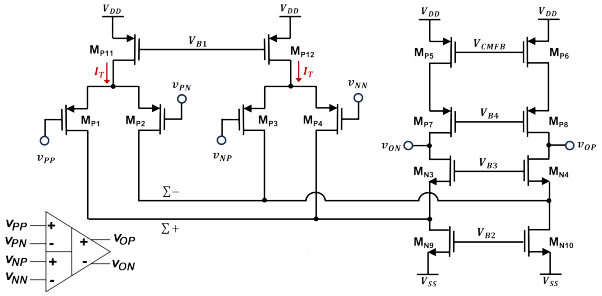

Fig. 3. FDDA at the transistor level

The circuit was designed following the methodology presented in [7] for an inversion level of 10. High-threshold voltage (HVT) transistors were selected for the PMOS devices to better achieve the desired current levels; however, this choice impacts both power consumption and input noise, which will be discussed later. In Figure 3 transistors MP1-MP4 convert the voltage differences $v_{pp} - v_{pn}$ and $v_{np} - v_{nn}$ into current differences that are combined in $\sum+$ and $\sum-$ through direct and cross connections, producing a differential current that is amplified by the high-gain output circuit [6].

B. Common-Mode Feedback (CMFB) and bias circuit

To ensure stable operation and correct the common-mode output levels, a common-mode feedback (CMFB) circuit is integrated into the FDDA design, as shown in Figure 4. The CMFB circuit monitors the common-mode voltage of the output and adjusts the bias currents accordingly to maintain a stable operating point. This is particularly important in differential amplifiers, where mismatches and variations in process parameters can lead to imbalances in the output signal.

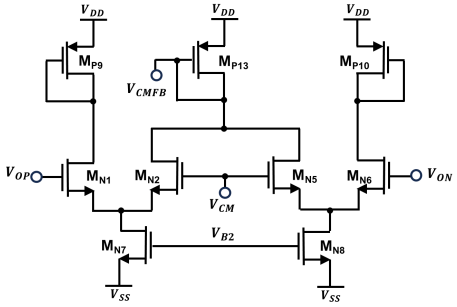

Fig. 4. Common-mode feedback circuit for proposed FDDA.

The biasing of the FDDA is achieved through the bias circuit in Figure 5, which provides a stable reference current to all stages of the amplifier. The bias circuit ensures the FDDA operates within its correct operating point to maximize its gain and bandwidth. It uses a reference current $I_{REF} = 2.5\mu A$ and series and parallel association of transistors, as well as matching-driven layout techniques to ensure consistent operation across a wide range of temperatures and process variations.

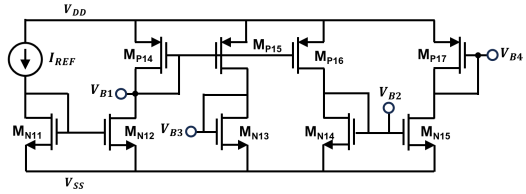

Fig. 5. Bias circuit for FDDA.

Table I summarizes the aspect ratios of transistors in the FDDA, CMFB, and bias circuits. Both PMOS and NMOS transistors use series and parallel associations with W=L=1μm to achieve these ratios.

III. Post-Layout Simulation Results

The FDDA circuit was designed and fabricated in 0.13 μm CMOS process from SkyWater as part of the first edition of the Universalization of IC Design from CASS (UNIC-CASS) Program. Figure 6 shows the Efabless [8] caravan chip top (left) and the FDDA circuit layout (right). At the time of

TABLE I
ASPECT RATIOS OF TRANSISTORS IN FDDA, CMFB AND BIAS CIRCUIT.

Transistor	W/L	Transistor	W/L
MP1-MP10	88/1	**MN1-MN6**	14/1
MP11-MP13	176/1	**MN7-MN10**	28/1
MP14-MP16	35/2	**MN11, MN12**	5/2
MP15	5/3	**MN13**	1/4
		MN14, MN15	5/2

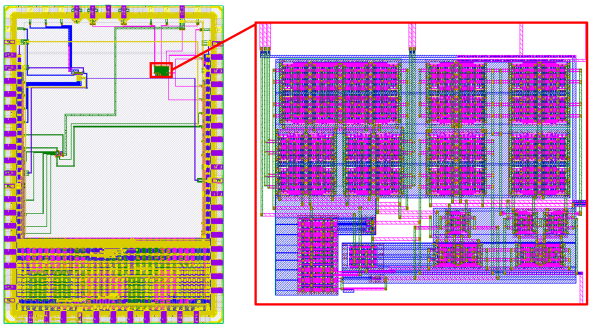

Fig. 6. Layout of Efabless caravan chip top [8] (left) and zoom in layout that includes FDDA, CMFB and bias circuit, 178 μm x 241 μm (right).

this writing, the chip has not yet arrived for bench measurements, therefore, the following results are from post-layout simulations in which parasitic resistances and capacitances were extracted from layout. Only the FDDA was integrated, allowing for its characterization and the configuration of the INA with different resistor ratios.

The FDDA achieved a DC gain of 72 dB, a gain-bandwidth product of 47.8 MHz, CMRR of 119.9 dB, phase margin of 55.46 degrees, and slew rate of 6.54 $V/\mu s$. The full frequency response can be observed in Figure 7. The PSRR is above 60 dB in the range from 1 kHz to 10 MHz, reaching 87.3 dB at 10 kHz and 90.7 dB at 1 MHz, which comprises the target operation range of the bioimpedance readout circuit, in which the FDDA-based INA will be implemented.

The FDDA-based INA simulations were conducted with a load capacitance of 1 pF, which reflects the maximum expected capacitance of the subsequent circuits in the readout system. Figure 8 shows the frequency response of the FDDA-based INA for three resistor ratios ($K_R = 5, 10, 20$). The circuit achieves a -3 dB bandwidth of 3.7 MHz for $K_R = 10$ which is sufficient to capture the full range of bioimpedance signals required for skin cancer detection. The FDDA-based INA presents consistent gain and phase performance across the desired frequency range, with slight variation depending on the selected gain.

The FDDA-based INA presents an 8.28 μV input offset voltage and an input-referred noise density of 275 $nV/\sqrt{Hz}$ at 1 kHz, as shown in Figure 10. While the noise level is acceptable, it could be lower; however, the use of HVT transistors may have contributed to the increase in noise.

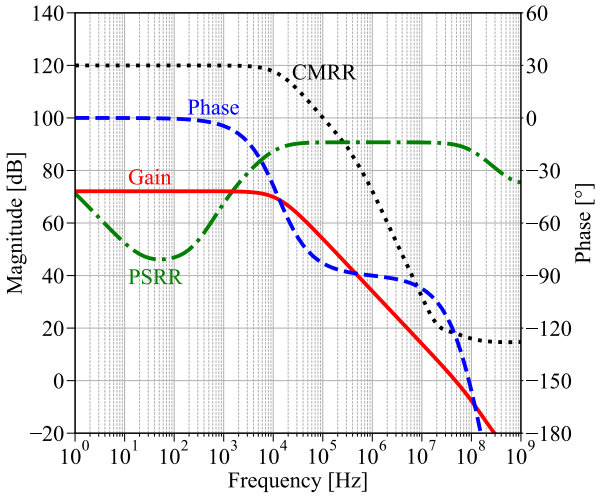

Fig. 7. Frequency response plot showing the gain, phase, CMRR, PSRR of the FDDA circuit.

TABLE II
TOTAL HARMONIC DISTORTION (THD) VALUES FOR THE FDDA-BASED INA ACROSS DIFFERENT FREQUENCIES AND GAINS.

Frequency	**THD [%]**		
K_R	5	10	20
1 kHz	0.066	0.075	0.101
10 kHz	0.079	0.087	0.099
100 kHz	0.081	0.148	0.352
500 kHz	0.386	1.156	3.399
1 MHz	1.041	3.122	8.323

To further evaluate the quality of the signal at the output, a 10 mV-amplitude differential sinusoidal waveform was applied to the input. Figure 9 shows the differential output results for three gains (with $K_R = 5, 10, 20$) and 50 kHz input signal. Table II presents the total harmonic distortion (THD) for the FDDA-based INA at different frequencies and gains. The circuit performs well with low THD at lower frequencies and lower gain. The highest THD is observed at 1 MHz for $K_R = 20$, however, the system is primarily intended to operate at lower gains (up to 10 V/V), where the THD remains within acceptable limits.

In comparison to other state-of-the-art FDDA designs listed in Table III, this work achieves a superior balance between DC gain (72 dB) and low noise, with a power consumption of 219.6 μW, which is competitive when considering the high CMRR of 119.9 dB at 1 kHz. Additionally, the GBW of 47.77 MHz is only surpassed by Matthus's design [10] which consumes more than ten times the power.

IV. CONCLUSION

This paper presented an FDDA-based INA as part of a bioimpedance readout circuit for skin cancer detection. The open-source design flow using the SkyWater 0.13 μm CMOS process demonstrates that high-performance biomedical circuits can be successfully developed using open-source tools

TABLE III
PERFORMANCE COMPARISON OF THE FDDA CIRCUIT.

Parameter	R. Ravasz, et al. [9] [m]	C. D. Matthus, et al. [10] [m]	F.Khateb, et al. [5] [s]	This work [p]
Process [μm]	**0.13**	**0.18 BCD**	**0.18**	**0.13 Open Source**
V_{DD} **[V]**	0.4	1.8	0.5	1.8
A_{vo} **[dB]**	43.5	46	61.4	72
GBW [MHz]	0.7586	400[+]	0.00698	47.77
Phase margin [°]	-	-	60.2	55.46
Slew rate [$V/\mu s$]	-	-	0.006	6.54
CMRR [dB]	91.2 @ 1 kHz	190 @ 10 kHz	100.3@ 1 Hz	119.9 @ 1 kHz
PSRR [dB]	73 @ 1 kHz	-	127.8 @ 1 Hz	67.49 @ 1 kHz; 87.32 @ 10 kHz
Input Noise [$\mu V/\sqrt{Hz}$] @ 1 kHz	-	0.08 [s]	1.2	0.275
Power [μW]	23.92[*]	3000	0.2465[*]	219.6[*]
C_L **[pF]**	-	-	30	1

[s,p,m] Schematic simulation, post-layout simulation, measurements.
[+] Gain-bandwidth product calculated by DC gain and 3 dB-bandwidth.
[*] Calculated by $V_{DD} \times I_{DD}$.

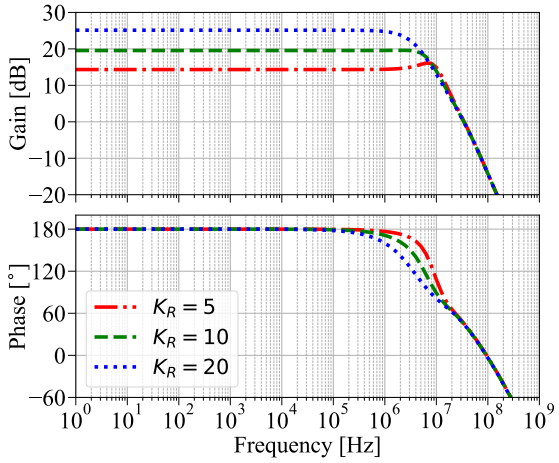

Fig. 8. Gain and phase response of the FDDA-based INA for different gains ($K_R = 5, 10, 20$)

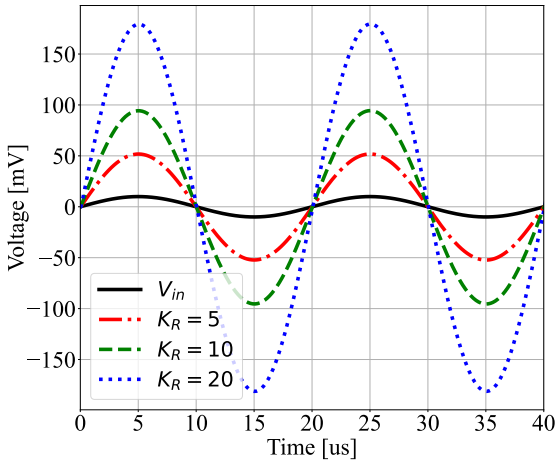

Fig. 9. Time-domain response of the FDDA-based INA for different gain settings (K_R =5,10,20), showing the differential output voltage (V_{OUT}) for each configuration in response to the input signal (V_{IN}).

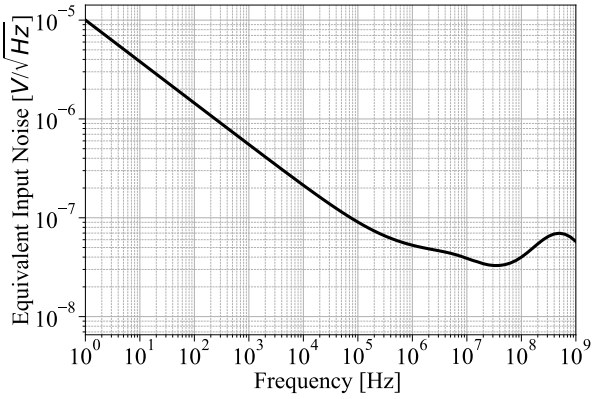

Fig. 10. Equivalent input noise spectral density of the FDDA-based INA across the frequency range.

from design to tape-out. The FDDA-based INA delivers high gain, wide bandwidth, low noise, and excellent common-mode rejection, making it well-suited for amplifying the small differential signals required in this application. Post-layout simulation results validate the INA's performance, paving the way for its integration into a complete bioimpedance measurement system. The FDDA circuit has been sent to tape-out and is currently in the final stage of fabrication. Future work will involve the tape-out of the full readout circuit (Figure 1) in an ASIC and experimental validation of the INA's performance in real-world bioimpedance applications.

ACKNOWLEDGMENT

The authors gratefully acknowledge the IEEE Circuits and Systems Society (CASS) for supporting the Universalization of IC Design program (UNIC-CASS). This research was funded by the Brazilian government agencies CAPES (Finance Code 001) and CNPq.

REFERENCES

[1] S. M. Moqadam, P. K. Grewal, Z. Haeri, P. A. Ingledew, K. Kohli, and F. Golnaraghi, "Cancer detection based on electrical impedance spectroscopy: A clinical study," *Journal of Electrical Bioimpedance*, vol. 9, no. 1, pp. 17–23, 2018.

[2] P. Kassanos, I. F. Triantis, and A. Demosthenous, "A CMOS magnitude/phase measurement chip for impedance spectroscopy," *IEEE Sensors Journal*, vol. 13, no. 6, pp. 2229–2236, 2013.

[3] P. Kassanos, L. Constantinou, I. F. Triantis, and A. Demosthenous, "An integrated analog readout for multi-frequency bioimpedance measurements," *IEEE Sensors Journal*, vol. 14, no. 8, pp. 2792–2800, 2014.

[4] H. Alzaher and M. Ismail, "A CMOS fully balanced differential difference amplifier and its applications," *IEEE Transactions on Circuits and Systems II: Analog and Digital Signal Processing*, vol. 48, no. 6, pp. 614–620, 6 2001. [Online]. Available: http://ieeexplore.ieee.org/document/943332/

[5] F. Khateb, T. Kulej, M. Kumngern, and C. Psychalinos, "A compact power-efficient 0.5V fully differential difference amplifier," *AEU - International Journal of Electronics and Communications*, vol. 105, pp. 71–77, 6 2019.

[6] E. Sackinger and W. Guggenbuhl, "A versatile building block: the CMOS differential difference amplifier," *IEEE Journal of Solid-State Circuits*, vol. 22, no. 2, pp. 287–294, 4 1987. [Online]. Available: http://ieeexplore.ieee.org/document/1052715/

[7] M. C. Schneider and C. Galup-Montoro, *CMOS analog design using all-region MOSFET modeling*. Cambridge University Press, 1 2010.

[8] Efabless, "Caravel Analog User," 2024. [Online]. Available: https://github.com/efabless/caravel_user_project_analog

[9] R. Ravasz, M. Potočný, D. Arbet, M. Kováč, D. Maljar, L. Nagy, and V. Stopjaková, "Measurement Approach to Evaluation of Ultra-Low-Voltage Amplifier ASICs," *Measurement Science Review*, vol. 24, no. 1, pp. 9–16, 2 2024.

[10] C. D. Matthus, S. Buhr, M. Kreibig, and F. Ellinger, "High Gain and High Bandwidth Fully Differential Difference Amplifier as Current Sense Amplifier," *IEEE Transactions on Instrumentation and Measurement*, vol. 70, 2021.